"Mircea cel Batran" Naval Academy Scientific Bulletin, Volume XV – 2012 – Issue 2
Published by "Mircea cel Batran" Naval Academy Press, Constanta, Romania

HOW DOES THE ASYMMETRY COEFFICIENTS DISTINGUISH BETWEEN THE ORDERED OR CHAOTIC ORBITS OF A DYNAMICAL SYSTEM?

Dumitru DELEANU[1]
[1]Professor, Department of Mathematical Sciences, Maritime University of Constanta

Abstract*: The "Asymmetry coefficients" due to Waz et al have been proved by them in the case of the damped driven pendulum to distinguish between regular and chaotic orbits of a dynamical system. The test is equally applicable to data generated from maps, ordinary differential equations and to the experimental data and have some useful advantages when is compared with other tests for chaos. Because we have thought that other numerical studies are necessary for a better understanding of the behavior of these indicators we applied them to other dynamical system, well-studied in the literature by means of accepted tools. In this paper we investigate the performance of the "Asymmetry coefficients" when applied to a coupled-single species population map and to the motion of a square prism in cross-flow and show that the test is straightforward to implement and performs extremely well.*
Keywords*: indicator of chaos, dynamical system, ordered and chaotic orbits*

1. INTRODUCTION

Chaotic behavior often occurs in engineering's and natural systems. From compound pendulums to dripping faucets, from predator-prey ecologies to measle epidemics, from oscillatory chemical reactions to irregular beats of a chicken heart, the underlying mechanism of chaos have been details in hundreds of papers and experiments.

In the past chaotic behavior has been seen as irregular or unpredictable and was often attributed to random external influences. Further studies have shown that chaotic behavior is deterministic, and is a typical characteristic of nonlinear systems.

There are various methods/indicators for detecting chaos. The first in chronological order were time series (observation of the state variables), phase portraits, Poincare section of surface, Lyapunov exponents, bifurcation diagram, Fourier spectra, Kolmogorov entropy, correlation dimension and so on. Some of them are rarely used, because they are difficult to apply in practical systems

The recent developed methods seem to be more efficient and faster than the older ones, especially for systems with many degrees of freedom. Most of these methods/indicators are based on deviation vectors, for instance, the spectra of stretching numbers (SSN), the alignment indices (GALI, SALI), the average power law exponent (APLE), the fast Lyapunov indicator (FLI), the mean exponential growth of nearby orbits (MEGNO) etc. All these methods require the numerical integration of the equations of motion together with the so-called variational equations, which govern the time evolution of deviation vectors. Usually, these techniques require quite a lot of computing time. To overcome this difficulty some symplectic or non-symplectic integrators have been proposed [1-8].

Unfortunately, in practical applications only a limited set of the observational data is available and the task of determining whether the observed motion is chaotic or regular may be difficult and the uncertainty of the results rather large. For this situation, other tests have been introduced in the literature [9-12]. One of them has been proposed by Gottwald and Melbourne, and returns 0 for a non-chaotic system and 1 for a chaotic system. In 2009, Waz et al proposed an alternative, very simple and related to the observational data, statistical indicator of chaos. In their approach the values of a time dependent function describing the studied motion are recorded in a sequence of time intervals and each of these recordings are considered statistical distributions. Then, the "asymmetry coefficients" of these distributions are defined and their behavior for ordered and chaotic orbits is analyzed. Their indicator was applied only in the simple case of the damped driven pendulum. We have thought that other numerical studies are necessary for a better understanding of this indicator so, in the present paper, we applied it to a coupled-single species population map and to the motion of a square prism in cross-flow.

The organization of rest of the paper is as follows. Section 2 contains the details of the method proposed by Waz et al. All calculations and numerical results are given in Section 3. The final remarks and conclusions are presented in Section 4.

2. METHOD OF THE ASYMMETRY COEFFICIENTS

For the sake of completeness let us briefly recall the definition of the "Asymmetry coefficients" and their behavior for regular and chaotic orbits. The interested reader can consult [9] to have a more detailed description of the method.

Let $X(t)$ be a function characterizing the motion we are going to analyze. Usually, in practical applications, $X(t)$ is known as a part of the solution of a differential systems of equations or from experimental measurements, so its values are given in a discrete set of points $\{X_i\}$.

Let us define a time-series $X_k(t) = \{X(t), t \in (T_0, T_{f\,k})/\, k = 1,2,..,K\}$ with a fixed T_0 and $T_{f1} < T_{f2} < ... < T_{fK}$. The terms of the series are treated as statistical distributions. The starting time T_0 and the final one T_{fK} denote the beginning and the end of the *k*-th distribution $X_k(t)$ and $\Delta T_k = T_{fk} - T_0$ is its length.

The asymmetry coefficients of the discrete *k*-th distribution X_k are defined as:

$$A_q(k, N_k) = S(k, N_k) \cdot \sum_{i=1}^{N_k} \left(X_{t_i^k} + c \right) \left[\frac{t_i^k - M_1(k, N_k)}{\sqrt{M_2(k, N_k) - M_1^2(k, N_k)}} \right]^q$$

$$S(k, N_k) = \left[\sum_{i=1}^{N_k} \left(X_{t_i^k} + c \right) \right]^{-1} \tag{1}$$

$$M_n(k, N_k) = S(k, N_k) \cdot \sum_{i=1}^{N_k} \left(X_{t_i^k} + c \right) \cdot \left(t_i^k \right)^n, \; n \in \{1,2\}$$

$q = 2j+1,\ j = 1,2,3,\ldots$, and *c* is a constant. N_k is the number of points in the *k*-th distribution, i.e. $t_i^k = \tau_i$, $i = 1,2,\ldots,N_k$, $k = 1,2,\ldots,K$, with $t_1^k = T_0, t_{N_k}^k = T_{f_K}$, $N_1 < N_2 < \ldots < N_K$. Since T_0 is the same for all *k* the length of the *k*-th distribution is proportional to N_k.

Waz et al [9] shown that the qualitative results are the same for all *c* chosen so $X_k(t) + c \geq 0$. Using the damped driven pendulum, Waz et al demonstrated that for a periodic motion the asymmetry coefficients approach 0 while T_f approaches infinity. For a chaotic orbit no regular asymptotic behaviour was observed.

3. NUMERICAL RESULTS

3.1. A coupled-single species population map

A general model for the growth of a single-species population with non-overlapping generations is

$$N_{t+1} = f(N_t) = \lambda N_t (1 + a N_t)^{-b} \tag{2}$$

where N_t and N_{t+1} are the populations in successive generations, λ is the finite rate of increase and a, b are constant defining the density-dependent feedback term. Let us consider the following coupled system

$$N_{t+1} = f(N_t) + c\left(f(M_t) - f(N_t)\right),\ M_{t+1} = f(M_t) + c\left(f(N_t) - f(M_t)\right) \tag{3}$$

This system can be clearly interpreted in populations light dynamics. One can think of $f(N_t)$ and $f(M_t)$ as simulating the population dynamics of a particular species at two adjacent locations. If the species can migrate in both directions within the time intervals between the stages of their reproduction and death then $c \in [0,1]$ represents the fraction of these species which migrate to the neighboring location [13, 14].

The effect of coupling consists in a rich dynamic behavior. A detailed analysis has been performed for $b = 6$, $\lambda = 60$, $a = 0.003$ and for four values of *c*. For $c = 0.0075$ the solution is periodic with period $T = 8$, for $c = 0.0115$ it is a quasi-periodic while for $c = 0.0005$ and $c = 0.25$ the solutions are chaotic (see Figure 1).

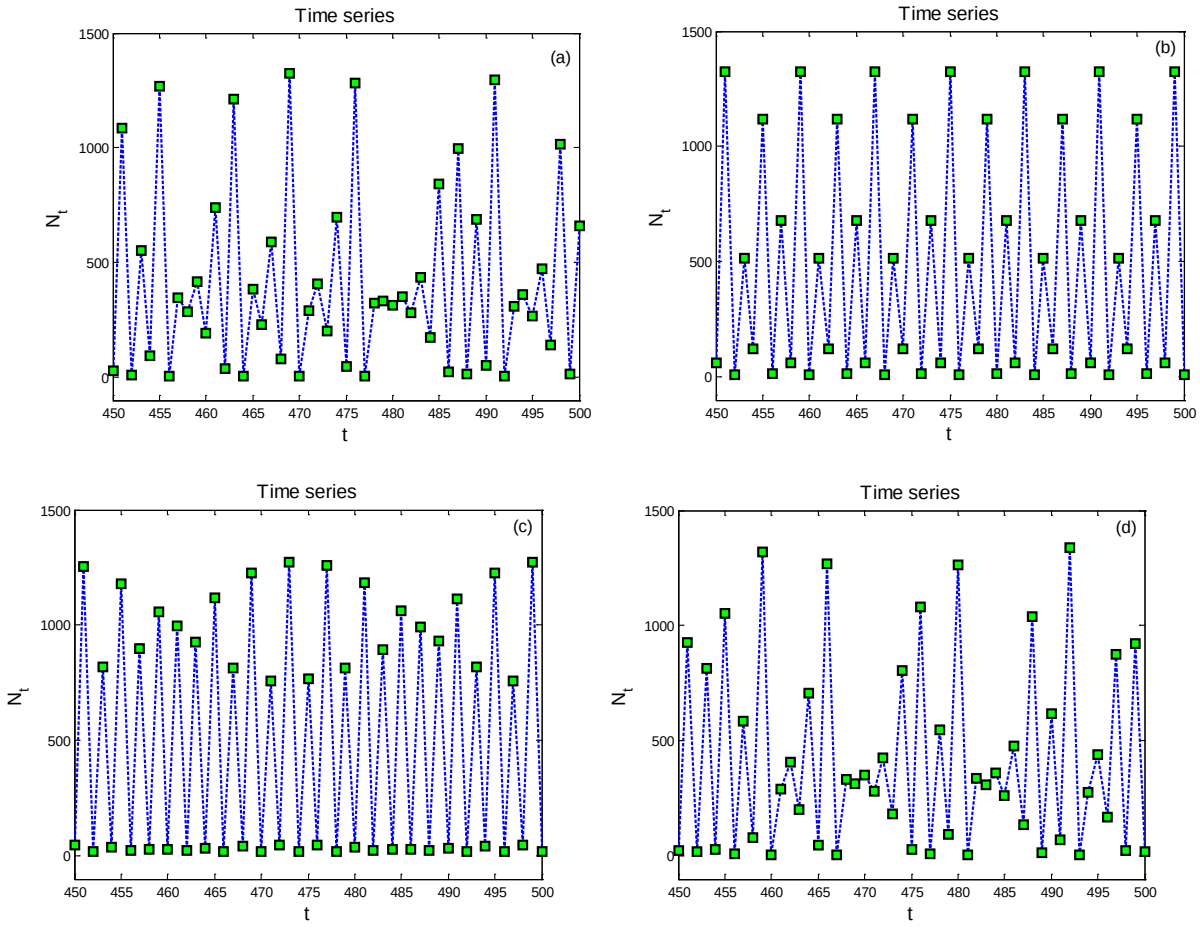

Figure 1: Time series for component N_t

a) $c = 0.0005$; b) $c = 0.0075$; c) $c = 0.0115$; d) $c = 0.25$

The calculations of asymmetry coefficients have been performed for first 50,000 iterations. The origin of each distribution corresponds to the initial time $T_0 = 1$ whereas the final points of each distribution have been selected as $T_{f\,k} = 10\,k,\, k = \overline{1, 5000}$. *c* was fixed at 10. In addition, $X(t) = N_t$.

Figure 2 presents the asymmetry coefficient A_3 as function of time, i.e. the lengths of the distributions. For an ordered orbit (periodic or quasiperiodic) the coefficient A_3 converges to zero, after a short transition period. An irregular behavior of A_3 can be seen for the chaotic orbits. The qualitative results are the same for other asymmetry coefficients (A_5, A_7 and so on) and for $X(t) = M_t$. The right panel shows an enlargement of left panel for the first 8,000 iterations.

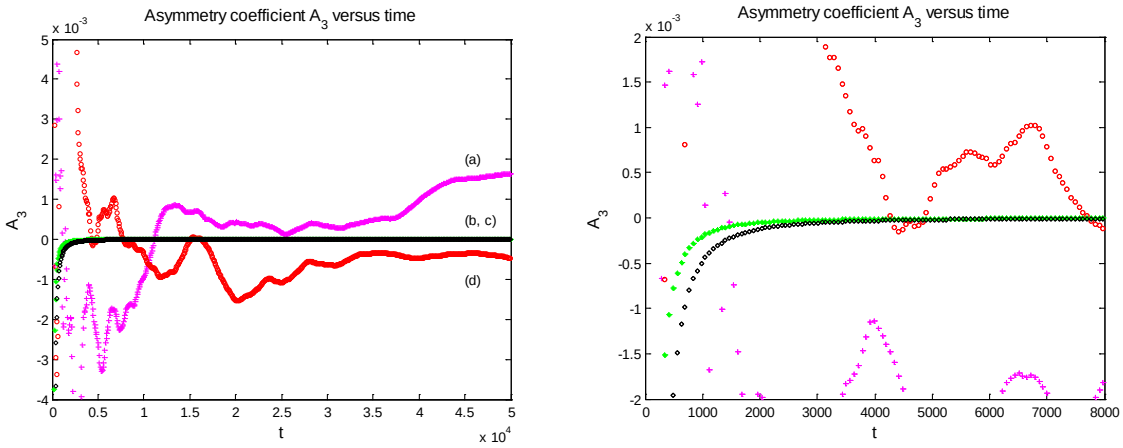

Figure 2: Dependence of asymmetry coefficient A_3 with time

Table 1 presents the mean values of A_q, $q = 3, 5, 7$, calculated for *t* in the range from 40,000 to 50,000. This range was used throughout the paper.

	(a)	(d)	(b)	(c)
A_3	0.0015	-0.00039	$-1.0266 \cdot 10^{-7}$	$-2.4791 \cdot 10^{-7}$
A_5	0.0064	-0.0020	$-6.1522 \cdot 10^{-7}$	$-1.4867 \cdot 10^{-6}$
A_7	0.0224	-0.0073	$-2.7688 \cdot 10^{-6}$	$-6.6871 \cdot 10^{-6}$

Table 1: The mean values of A_q, $q = 3, 5, 7$

A better separation of these plots can be realized showing the separation of $\lg|A_q|$ with time (see Figure 3). It is obvious that $\lg|A_3|$ converges to large negative values for periodic orbits and behaves randomly for chaotic orbits. In fact, for all the examples discussed in the paper these features have remained unchanged so, in the following, we were interested only in a numerical comparison of asymmetry coefficients' mean values.

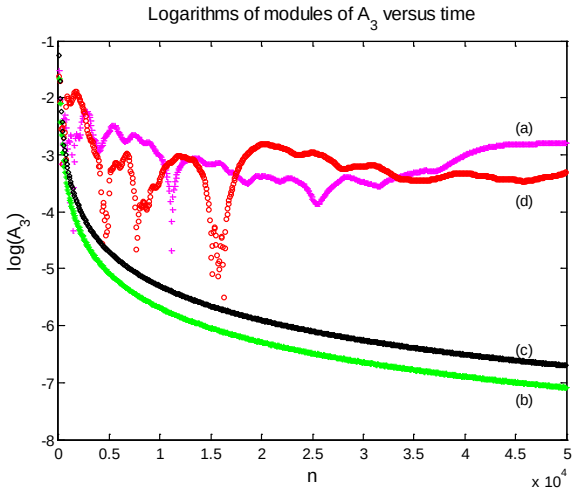

Figure 3: Dependence of the logarithms of asymmetry coefficient A_3 with time

3.2. Motion of a square prism in cross-flow

Let a square prism be supported by a non-linear spring with a linear viscous damper. The prism is assumed to be excited harmonically and kept in a steady fluid flow, perpendicular to its displacement. The motion is governed by differential equation:

$$m\frac{d^2y}{dt^2}+c\frac{dy}{dt}+k_1 y+k_3 y^3=F\cos(\omega t)+F_L \tag{4}$$

where y is the displacement, m is the mass of the prism, c is the linear viscous damping coefficient, k_1 and k_3 are, respectively, the coefficients of linear and cubic stiffness, F and ω are, respectively, the amplitude and the frequency of the harmonic force, t is the time and F_L is the lift force given by

$$F_L=\frac{1}{2}\rho D L V^2\left(\frac{B_1}{V}\frac{dy}{dt}+\frac{B_3}{V^3}\left(\frac{dy}{dt}\right)^3\right) \tag{5}$$

In (5), ρ is the flow density, D and L are the prism's dimensions, V is the flow velocity whereas B_1 and B_3 are coefficients characterizing the geometry of the bluff body [15]. Using the non-dimensional quantities

$$x=y/L,\ U=V/\omega d,\ \tau=\omega t,\ F_a=F/m\omega^2 L,\ \ \xi=c/m\omega,\ \omega_n^2=k_1/m,\ \gamma_1=k_1/m\omega^2,$$

$$\gamma_3=k_3L^2/m\omega^2,\ \beta=\rho D L^2/m,\ \ \zeta_1=-\beta B_1 U/2,\ \zeta_3-\beta B_3/2U,\ \zeta_a=\zeta+\zeta_1$$

equation (4) becomes:

$$\frac{d^2x}{d\tau^2}+\zeta_a\frac{dx}{d\tau}+\zeta_3\left(\frac{dx}{d\tau}\right)^3+\gamma_1 x+\gamma_3 x^3=F_a\cos\tau \tag{6}$$

Equation (5) was numerically integrated in the interval $\tau\in[0,\ 200\pi]$ with zero initial conditions for the following parameters: $B_1=2.7,\ B_3=-31.0,\ \zeta=0.1,\ \ \zeta_1=\zeta_3=1.0,\ \beta=0.12256$ and $F_a=10.0$. The non-dimensional flow velocity was taken as the bifurcation parameter and varied from 5 to 14. This choice is based on the results obtained in [15]. The time step for the integration was taken as $\Delta\tau=T/256$ ($T=2\pi$ is the period of the harmonic excitation force $F_a\cos\tau$) so we get a number of 25,601 points of integration.

For small values of *U* the prism executes periodic oscillations with period 1. As *U* increases and reaches a value of 8.41 the period 1 orbit bifurcates into a period 2 orbit. Further increases in *U* result in a series of period 4 orbit (*U* = 8.9), period 8 orbit (*U* = 8.94) and so on. Starting with *U* = 8.96, the orbit becomes chaotic. Within the chaotic window narrow periodic windows appear. For our purposes we selected four values of *U*. Thus, for *U* = 8.5 and *U* = 10.3 we get a period 2 orbit and a period 3 orbit, respectively, whereas for *U* = 9.2 and *U* = 12.3 the orbits are chaotic (see Figure 4). The points of the Poincare map corresponding to one period of harmonic excitation are also plotted in Figure 4 and are indicated by a green square.

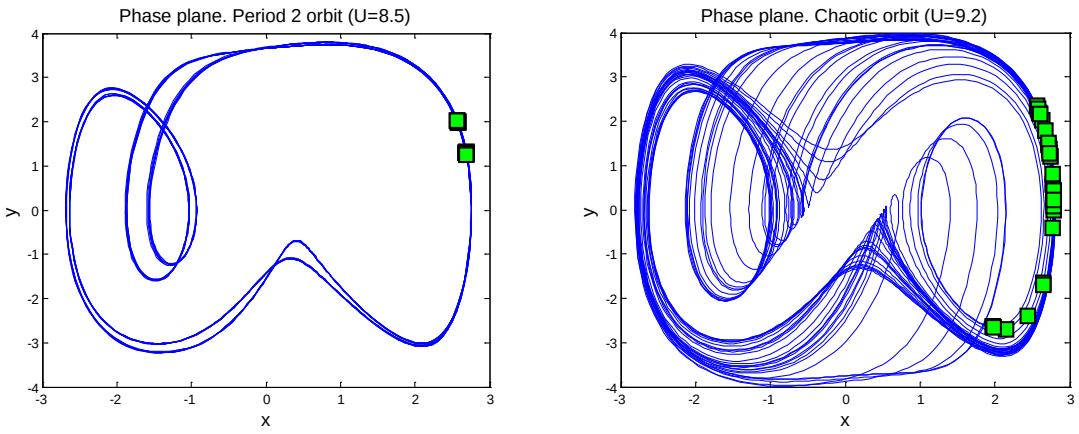

(a) (b)

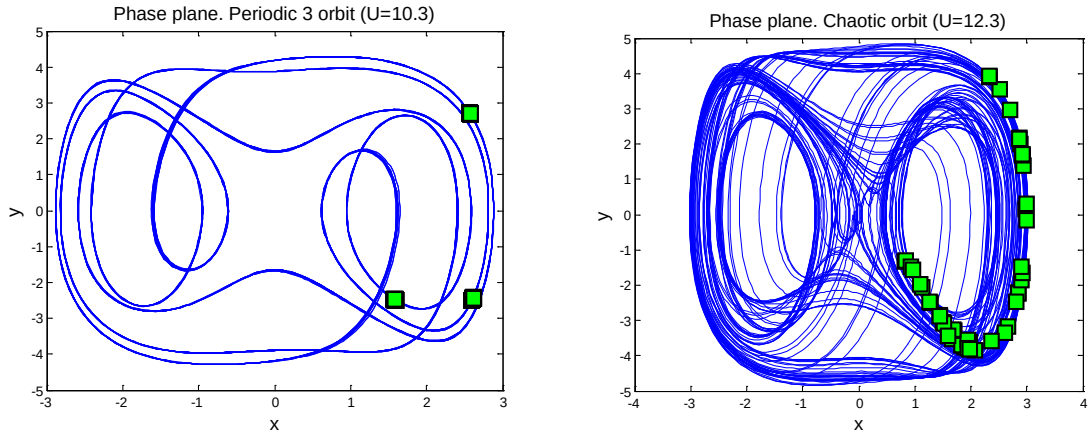

Figure 4: Phase plane for the square prism in cross-flow

a) U = 8.5; b) U = 9.2; c) U = 10.3; d) U = 12.3

To avoid the initial transition we took as origin of each distribution time $T_0 = 5602 \cdot \Delta\tau$ so we used practically 20,000 values in the time series. The ends of the distributions have been selected as $T_{fk} = 10 \cdot k,\ k = \overline{1, 2000}$. The asymmetry coefficients have been calculated with c = 6 and $X(\tau) = x(\tau)$. Figure 5 presents the behavior of $\lg|A_3|$. The two curves corresponding to periodic orbits converge to large negative values and are well separated from the two curves associated to the chaotic orbits.

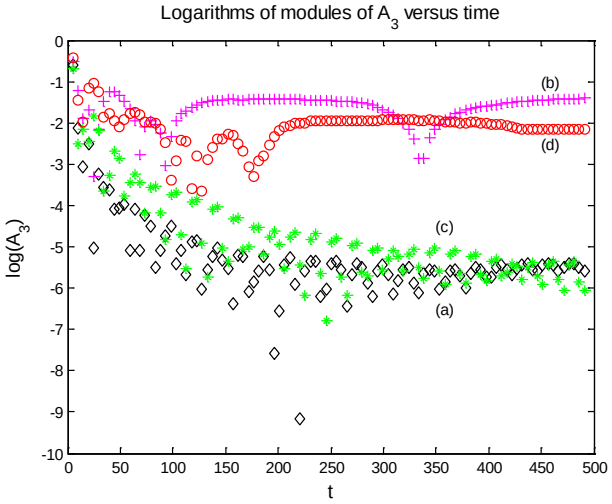

Figure 5: Dependence of the logarithms of asymmetry coefficient A_3 with time

3.3. Parametric studies

In this section, we have performed a number of numerical simulations in order to obtain an idea about the influence of some parameters, like constant *c* or the number of measurement points, on the behavior of the asymmetry coefficients. To this purpose, we worked with the coupled-single species population map.

3.3.1. Dependence on *c*

As we have already mentioned, the qualitative results concerning the asymmetry coefficients remain unchanged no matter which value for *c* is considered. To prove this, Table 2 presents the mean values of A_7 calculated with different values of *c*. It is obvious that, in every case, the values of A_7 for chaotic orbits differ by few orders of magnitude from those corresponding to periodic orbits. In addition, the values of A_7 become greater and greater while $\min_t(N_t + c)$ tends to zero.

	(a)	(b)	(c)	(d)
c = 0	0.0229	$-2.8252\cdot10^{-6}$	$-6.8154\cdot10^{-6}$	- 0.0075
c = 50	0.0205	$-2.5639\cdot10^{-6}$	$-6.2185\cdot10^{-6}$	- 0.0067
c = 250	0.0144	$-1.8715\cdot10^{-6}$	$-4.6052\cdot10^{-6}$	- 0.0047
c = 1250	0.0058	$-7.9625\cdot10^{-7}$	$-2.0047\cdot10^{-6}$	- 0.0019
c = 3000	0.0028	$-3.9705\cdot10^{-7}$	$-1.0083\cdot10^{-6}$	- 0.0009
c = 10000	0.0009	$-1.3211\cdot10^{-7}$	$-3.3744\cdot10^{-7}$	- 0.0003

Table 2: Dependence on constant *c* of the asymmetry coefficient A_7

3.3.2. Dependence on the number of measurement points

Because a periodic motion is self-similar over sufficiently large intervals of time, it is expected that $A_q,\ q = 3, 5, 7, \ldots$ approach 0 while number of measurement points N (or number of iterations for maps) tends to infinity. In the same time, for a chaotic motion no regular asymptotic behavior is expected. To verify this statement, we significantly increased the number of iterations. Table 3 presents the effect of increasing N from 50,000 to 500,000.

N	(a)	(b)	(c)	(d)
50,000	0.0229	$-2.8432\cdot10^{-6}$	$-6.8163\cdot10^{-6}$	-0.0075
100,000	0.0028	$-7.1140\cdot10^{-7}$	$-1.7055\cdot10^{-6}$	0.0024
500,000	$-7.8785\cdot10^{-4}$	$-2.8591\cdot10^{-8}$	$-6.8255\cdot10^{-8}$	$-7.9033\cdot10^{-5}$

Table 3: Dependence on the number of iterations of the asymmetry coefficient A_7

In Figure 6 we report the results of the numerical computation for N = 500,000. Both the Table 3 and the Figure 6 agree very well with our expectations.

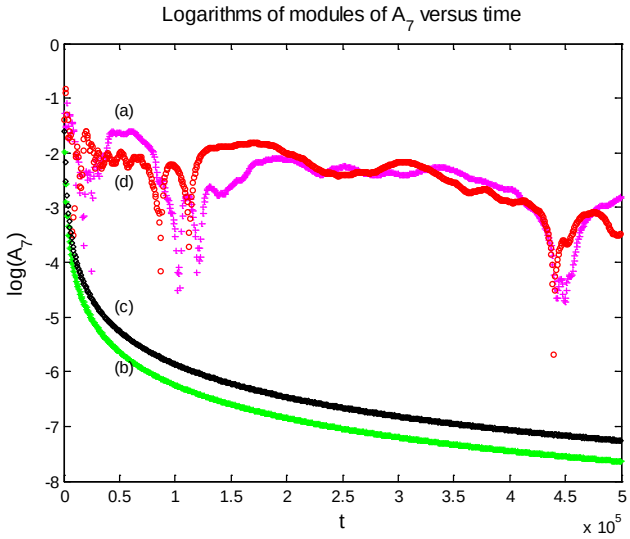

Figure 6: Dependence of the logarithms of asymmetry coefficient A_7 with time

4. Conclusions

The goal of this work was to apply the "Asymmetry coefficients" method for distinguishing between ordered and chaotic orbits in the case of discrete or continuous-time dynamical systems. We investigated the coupled-single species population map and the motion of a square prism in cross-flow.

The main conclusions of the study are:

a) For an ordered orbit (periodic or quasi-periodic) the asymmetry coefficients converge to zero whereas for a chaotic orbit no sign of convergence can be observed;

b) If the logarithms of asymmetry coefficients are plotted instead, a convergence to large negative values is observed for ordered orbits and no convergence in case of chaos. The separation between the two types of curves becomes more evident by the time passes (or number of iterations grows for maps);

c) The qualitative results concerning the asymmetry coefficients remain unchanged no matter which value for *c* is considered (which ensure the condition $X_k(t)+c \geq 0$, *X(t)* being the analyzed function) . The values of asymmetry coefficients become greater and greater while $\min_t\left(X(t)+c\right)$ tends to zero;

d) The method has a few advantages when compared with other similar methods. Thus:
   - the equations of the underlying dynamics do not need to be known;
   - the dimensionality of the vector field has not practical limitations;
   - the nature of the dynamical system is irrelevant for the implementation of the test. The test is applicable to data generated from maps, ordinary differential equations and to the experimental data;
   - the computational effort is of low cost, both in terms of programming effort and in terms of computational time;

e) For numerical integrations we have used modern software, i.e. MatLab package, where the possibility of occurring of round off error be minimum;

REFERENCES

1. Deleanu D., *New applications of Fast Lyapunov Indicator for discrete_time dynamical systems*, Constanta Maritime University Annals, Vol 15, 2011
2. Deleanu, D., *Dynamic Lyapunov Indicator : a practical tool for distinguishing between ordered and chaotic orbits in discrete dynamical systems* , Proceedings of the 10th WSEAS International Conference on Non-Linear Analysis , Non-Linear Systems and Chaos (NOLASC'11), Iasi, Romania, July 1-3, 2011, pp. 117-122.
3. Froeschle, C., Gonczi, R., Lega, E., *The Fast Lyapunov Indicator: A simple tool to detect weak chaos, Application to the structure of the main a steroidal belt,* Planet. Space Sci., Vol 45, pp 881-886, 1997.
4. Maffione, N., Darriba, L., Cincotta, P., Giordano, C., *A comparison of different indicators of chaos based on the deviation vectors,* Celest. Mech. Dyn. Astron., Vol 111, pp 285-307, 2011.
5. Saha, L.M., Tehri, R., *Application of recent indicators of regularity and chaos to discrete maps,* Int. J. of Appl. Math. and Mech., Vol 6(1), pp 86-93, 2010.
6. Saha, L.M., Budhraja, M., The largest eigenvalue: An indicator of chaos, Int. J. of Appl. Math. and Mech., Vol 3(1), pp 71-71, 2007.
7. Skokos, C.H., *Alignment indices: a new, simple method for determining the ordered or chaotic nature of orbits*, J. Phys. A: Math. Gen., Vol 34, pp 10029-10043, 2001.
8. Voglis, N., Contopoulos, G., Efthymopoulos, C., *Method for distinguishing between ordered and chaotic orbits in four-dimensional maps*, Physical Review E., Vol 57, pp 372-377, 1998.
9. Waz, P., Waz, D.D*., Asymmetry coefficients as indicators of chaos*, Acta Physica Polonica, Vol 116, pp 987-991, 2009.
10. Gottwald, G.A., Melbourne, I, *A new test for chaos in deterministic systems*, Proc. Roy. Soc. London, Vol 460 , pp 603-611, 2004.
11. Gottwald, G.A., Melbourne, I, *Testing for chaos in deterministic systems with noise,* Physica D, Vol 212, pp 100-110, 2005.
12. Hu, J., Tung, W., Gao, J., Cao, Y., *Reliability of the 0-1 test for chaos,* Phys. Rev. E., Vol 72, 2005.
13. Hassell, M.P., *Density-dependence in single species populations,* The Journal of Animal Ecology, Vol 49(1), pp 283-295, 1975.
14. Laureano, R., Mendes, D.A., Ferreira, M.A.M., *Efficient synchronization of one-dimensional chaotic quadratic maps by different coupling terms*, Journal of Mathematics and Technology, Vol 17, pp 5-12, 2010.
15. Sekar, P., Narayanan, S., *Periodic and chaotic motions of a square prism in cross-flow,* Journal of Sound and Vibration, Vol 176(1), pp 1-24, 1994.